Constraining the Statistics of Population III Binaries

Athena Stacy[1]* and Volker Bromm[2]

[1] *NASA Goddard Space Flight Center, Greenbelt, MD 20771, USA*
[2] *Department of Astronomy and Texas Cosmology Center, University of Texas, Austin, TX 78712, USA*

ABSTRACT

We perform a cosmological simulation in order to model the growth and evolution of Population III (Pop III) stellar systems in a range of host minihalo environments. A Pop III multiple system forms in each of the ten minihaloes, and the overall mass function is top-heavy compared to the currently observed initial mass function in the Milky Way. Using a sink particle to represent each growing protostar, we examine the binary characteristics of the multiple systems, resolving orbits on scales as small as 20 AU. We find a binary fraction of $\sim 36\%$, with semi-major axes as large as 3000 AU. The distribution of orbital periods is slightly peaked at $\lesssim 900$ yr, while the distribution of mass ratios is relatively flat. Of all sink particles formed within the ten minihaloes, $\sim 50\%$ are lost to mergers with larger sinks, and $\sim 50\%$ of the remaining sinks are ejected from their star-forming disks. The large binary fraction may have important implications for Pop III evolution and nucleosynthesis, as well as the final fate of the first stars.

Key words: stars: formation - Population III - galaxies: formation - cosmology: theory - first stars - early Universe

1 INTRODUCTION

The period during which the first stars arose marked a pivotal turning point in the evolution of the Universe. The first stars, also known as Population III (Pop III), are believed to have formed at $z \gtrsim 20$ within dark matter (DM) minihaloes of 10^6 M$_\odot$ (e.g. Haiman et al. 1996; Tegmark et al. 1997; Yoshida et al. 2003). Afterwards they generated ionizing photons that contributed to the reionization of the Universe (e.g. Kitayama et al. 2004; Sokasian et al. 2004; Whalen et al. 2004; Alvarez et al. 2006; Johnson et al. 2007), while those Pop III stars that ended their lives as supernovae (SNe) contributed to the metallicity of the intergalactic medium (IGM; Madau et al. 2001; Mori et al. 2002; Bromm et al. 2003; Wada & Venkatesan 2003; Norman et al. 2004; Tornatore et al. 2007; Greif et al. 2007, 2010; Wise & Abel 2008; Maio et al. 2011; recently reviewed in Karlsson et al. 2012). This metal-enrichment and growing radiation background provided by the first stars determined the environment in which later stellar generations formed.

The mass of a given Pop III star plays the central role in determining how the star will influence its surroundings. For instance, more massive stars are more efficient in producing ionizing photons, per unit stellar mass, than low-mass

stars (Bromm et al. 2001; Schaerer 2002). Furthermore, non-rotating primordial stars with mass 140 M$_\odot < M_* < 260$ M$_\odot$ are believed to have exploded as pair-instability supernovae (PISNe; Heger & Woosley 2002), releasing the entirety of their metal content into the IGM and surrounding haloes, while stars within the range 15 M$_\odot < M_* < 40$ M$_\odot$ ended their lives as core-collapse SNe. On the other hand, non-rotating Pop III stars with main sequence masses in the range 40 M$_\odot < M_* < 140$ M$_\odot$ or $M_* > 260$ M$_\odot$ are expected to collapse directly into black holes (BHs), thus contributing no metals to their surroundings.

BH remnants of Pop III stars may emit copious amounts of radiation during subsequent mass accretion, however. While this radiation will heat and ionize its local surroundings, the X-ray component has a long mean-free path that allows it to ionize the IGM and minihalo gas as far as $10 - 100$ kpc away. This contributed to reionization, while the boosted electron fraction can catalyze the formation of additional H_2 molecules, mildly enhancing the global cooling and star-formation rate (e.g., Madau et al. 2004; Ricotti & Ostriker 2004; Kuhlen & Madau 2005; Haiman 2011; Jeon et al. 2012). Recent work has demonstrated that a BH remnant which has a stellar binary companion, giving rise to a high-mass X-ray binary (HMXB), will exert stronger feedback on its surroundings than an isolated BH (e.g., Mirabel et al. 2011; Jeon et al. 2012). This is because accretion onto

solitary BHs is more susceptible to feedback that in turn reduces the BHs accretion rate and luminosity (e.g. Johnson & Bromm 2007; Alvarez et al. 2009; Milosavljević et al. 2009), whereas the near-Eddington luminosity of a HMXB can persist through Roche lobe overflow. In this way the binary characteristics of Pop III stars will influence the nature of Pop III feedback. Also intriguing are observations indicating that ultra-luminous X-ray sources (ULXs), which may be accreting, intermediate-mass BHs, occur at a higher rate in less massive and lower-metallicity galaxies (e.g. Swartz et al. 2008). Recent modeling of binary system evolution over a range of metallicity also support a higher rate of ULX formation in lower-metallicity star clusters (Linden et al. 2010). We note that BH binaries are detectable in channels other than electromagnetic radiation. For instance, Kowalska et al. (2012) find that if Pop III stars left behind a significant BH population, then their gravitational wave (GW) emission will dominate the low-frequency (< 100Hz) spectrum as long as the Pop III binary fraction was at least 10^{-2}.

A binary companion can also influence a star's evolution during and after its main sequence (MS) stage, as well as the type of death the star will undergo (e.g. Wellstein et al. 2001; Petrovic et al. 2005, 2005b; Cantiello et al. 2007; de Mink et al. 2009; Langer 2012; Sana et al. 2012). For instance, massive stars that leave behind BH remnants may power collapsar gamma-ray bursts (GRBs; e.g. Woosley 1993; Lee & Ramirez-Ruiz 2006). However, this requires sufficient angular momentum in the Pop III progenitor for an accretion torus to form around the remnant BH. The progenitor star must also lose its hydrogen envelope to enable the relativistic jet to penetrate through and exit the star (e.g. Zhang et al. 2004, but see Suwa & Ioka 2011; Nakauchi et al. 2012). One way to fulfill both of these conditions is for the GRB progenitor to have a close binary companion that removes the hydrogen envelope due to the heating during a common-envelope phase (e.g. Lee et al. 2002; Izzard et al. 2004).

A star which receives mass from or merges with its binary companion potentially undergoes a process of 'rejuvenation' in which its central hydrogen abundance increases (e.g. Hellings 1983; Braun & Langer 1995; Dray & Tout 2007). This causes the star's apparent age to be less than its true age, and may lead the star to appear as a blue straggler on the Hertzsprung-Russel diagram (Langer 2012). Whether rejuvenation will result from mass transfer depends on the evolutionary stage of the binary components, and is not expected to occur if one of the members is already post MS. For instance, a star with an undermassive helium core may result instead (e.g. Braun & Langer 1995). Stellar mergers may furthermore lead to the generation of large-scale magnetic fields observed within massive MS stars (e.g. Donati & Landstreet 2009; Ferrario et al. 2009). In addition, while single stars must typically have masses $\gtrsim 20\,M_\odot$ to go through a Wolf-Rayet (WR) phase (Hamann et al. 2006), and even larger masses at lower metallicities (Meynet & Maeder 2005), a member of a close binary may become a WR star at a lower mass of $\sim 10\,M_\odot$ (e.g., Vanbeveren et al. 1998; Crowther 2007).

A star that gains mass from its binary companion through an accretion disk may spin up to critical rotation speed, and rapid rotation can alter a star's evolution in a number of ways (see, e.g., Stacy et al. 2011, 2012; Maeder & Meynet 2012; Yoon et al. 2012). Rotation will allow for rotationally induced mixing and possibly chemically homogeneous evolution (CHE). CHE, in turn, may lower the minimum mass at which a star will undergo a PISN to as low as $\sim 65\,M_\odot$ (e.g., Chatzopoulos & Wheeler 2012). If a rotating star instead leaves behind a BH remnant, a collapsar GRB may result even without a binary companion. This is because CHE may allow stars to bypass the red giant phase to become a WR star. This evolutionary path may furthermore allow the star to retain enough angular momentum to become a GRB (e.g. Yoon & Langer 2005; Woosley & Heger 2006). Rotationally induced chemical mixing will generally enhance a star's luminosity, temperature, and metal production, though this depends sensitively on the assumed magnetic field evolution within the star (e.g., Ekström et al. 2008; Yoon et al. 2012). Another possible consequence of both rotation and mass transfer is enhancement in surface nitrogen abundance (e.g. Ekström et al. 2008; Langer et al. 2008; Brott et al. 2011; Langer 2012).

Observations of massive stars in the Milky Way find that ~ 45-75% of O-stars have spectroscopic binary companions (Mason et al. 2009; Sana & Evans 2011), and calculations of binary evolution furthermore find that 20-30% of O-stars will merge with their companions (Sana et al. 2012). Binarity therefore plays a crucial role in the evolution of massive stars in the Milky Way. While similar observations cannot be made for Pop III stars, we may still study them numerically. Early computational studies of Pop III star formation indicated that they would grow to be highly massive ($\gtrsim 100\,M_\odot$; e.g. Abel et al. 2002; Bromm et al. 2002; Bromm & Loeb 2004; Yoshida et al. 2008), and that each minihalo would host only a single Pop III star. More recent work, however, has found that primordial star-forming gas will undergo continued fragmentation well after the initial star has formed. Pop III multiplicity has been found both in small-scale simulations that utilize idealized initial conditions (e.g. Machida et al. 2008, Clark et al 2008; 2011a), as well as simulations that are initialized on cosmological scales, (e.g. Turk et al. 2009; Stacy et al. 2010; Clark et al. 2011b, Greif et al. 2011, 2012) and also when accounting for radiative feedback (e.g. Smith et al. 2011; Stacy et al. 2012). Recent numerical advances have thus shown that the processes that lead to binary formation apply to both enriched and metal-free gas (e.g. Tohline 2002), and a new picture has emerged in which Pop III stars typically form in multiples and within disks.

In order to determine the role of multiplicity in Pop III evolution and feedback, in this study we aim to better constrain the nature of Pop III binaries. We do this through simulating a large cosmological box which contains approximately ten minihaloes in which primordial stars form by $z \simeq 20$. We examine the rate of binary formation and protostellar mergers, the typical characteristics of the binaries, and the overall mass function at this stage of evolution of the Pop III systems. Stars ejected from their Pop III cluster may stop accreting and remain low-mass and long-lived to the present day. Such stars may be observed in dwarf galaxies or the Milky Way halo, so we furthermore discuss the frequency of low-mass sink ejections in our suite of minihaloes. In Section 2 we describe our numerical methods, while we present our results in Section 3. We address our caveats in Section 4, and conclude in Section 5.
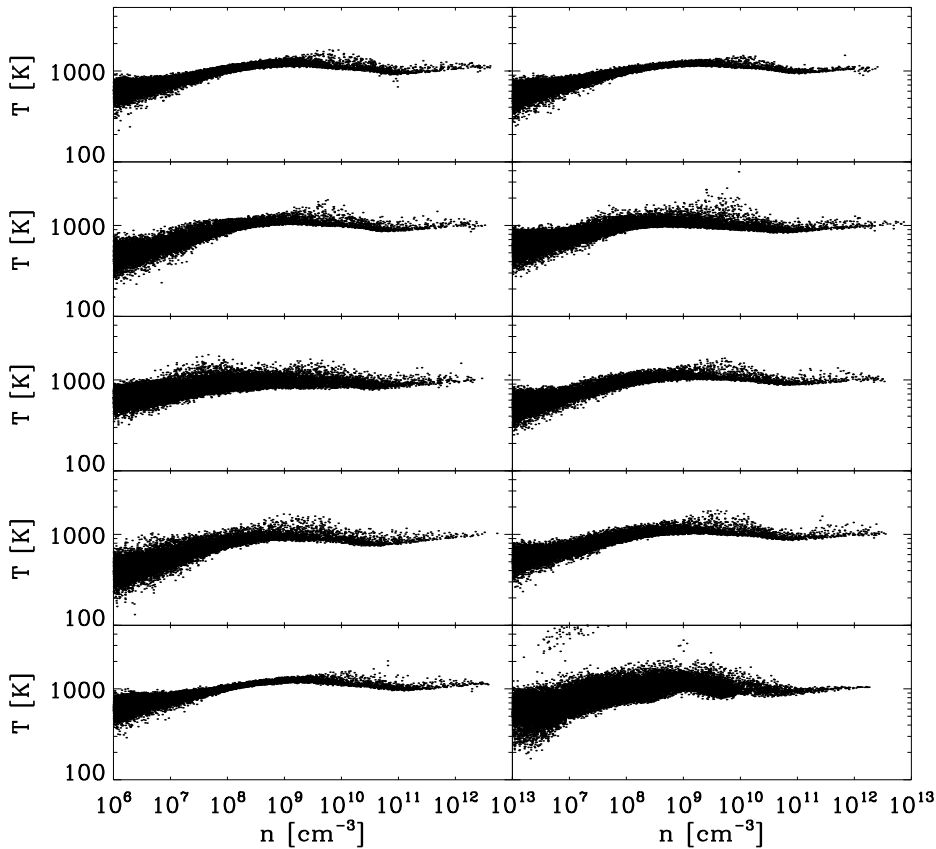
Figure 1. Temperature versus number density of the gas just prior to the formation of the first sink particle in each minihalo. The similarity in the early thermal evolution is striking. At $n > 10^8$ cm^{-3}, three-body reactions rapidly convert the gas into fully molecular form. The corresponding boost in H$_2$ cooling balances adiabatic heating, resulting in nearly isothermal evolution. H$_2$ line opacity will become important only at even higher densities, eventually causing deviations from the near-isothermality seen here.

2 NUMERICAL METHODOLOGY

2.1 Initial Setup

We perform our investigation using GADGET-2, a widely-tested three-dimensional N-body and SPH code (Springel 2005). We begin with a 1.4 Mpc (comoving) box containing 512^3 SPH gas particles and the same number of DM particles. The simulation is initialized at $z = 100$. Positions and velocities are assigned to the particles in accordance with a ΛCDM cosmology with $\Omega_\Lambda = 0.7$, $\Omega_M = 0.3$, $\Omega_B = 0.04$, $\sigma_8 = 0.9$, and $h = 0.7$. Each gas particle has a mass of $m_{sph} = 120$ M$_\odot$, while DM particles have a mass of $m_{DM} = 770$ M$_\odot$. Once a gas particle reaches a threshold density of 10^3 cm^{-3}, we employ 'marker sinks' instead of following these regions to increasingly higher densities. This allows us to efficiently evolve the entire box through a time period over which ten minihaloes form. Though the marker sinks are numerically similar to the protostellar sink particles to be described in Section 2.4, note that the marker sinks are implemented at much lower densities than the protostellar sink particles of the final highest-resolution calculations.

The location of the marker sinks coincides with the centers of the minihaloes. In particular, we locate the first ten sink particles which form within the first ten minihaloes. Once these positions are ascertained, the cosmological box is reinitialized at $z = 100$ for each individual minihalo, but with 64 'child' particles added around a 100-140 kpc region where the target halo will form. Larger regions of refinement are used for minihaloes whose mass originates from a larger area of the cosmological box. Particles at progressively larger distances from the minihalo are given increasingly larger masses, such that in the refined initial conditions there is a total of $\sim 10^7$ particles. The most resolved particles are of mass $m_{sph} = 1.85$ M$_\odot$ and $m_{DM} = 12$ M$_\odot$.

2.2 Cut-Out and Refinement Technique

The refined simulations are run until the gas reaches a density of 5×10^7 cm^{-3}. All particles beyond 10 physical pc are then removed from the simulation. Once the gas has reached these densities, this central star-forming region is gravitationally bound, and the effects of the outer minihalo
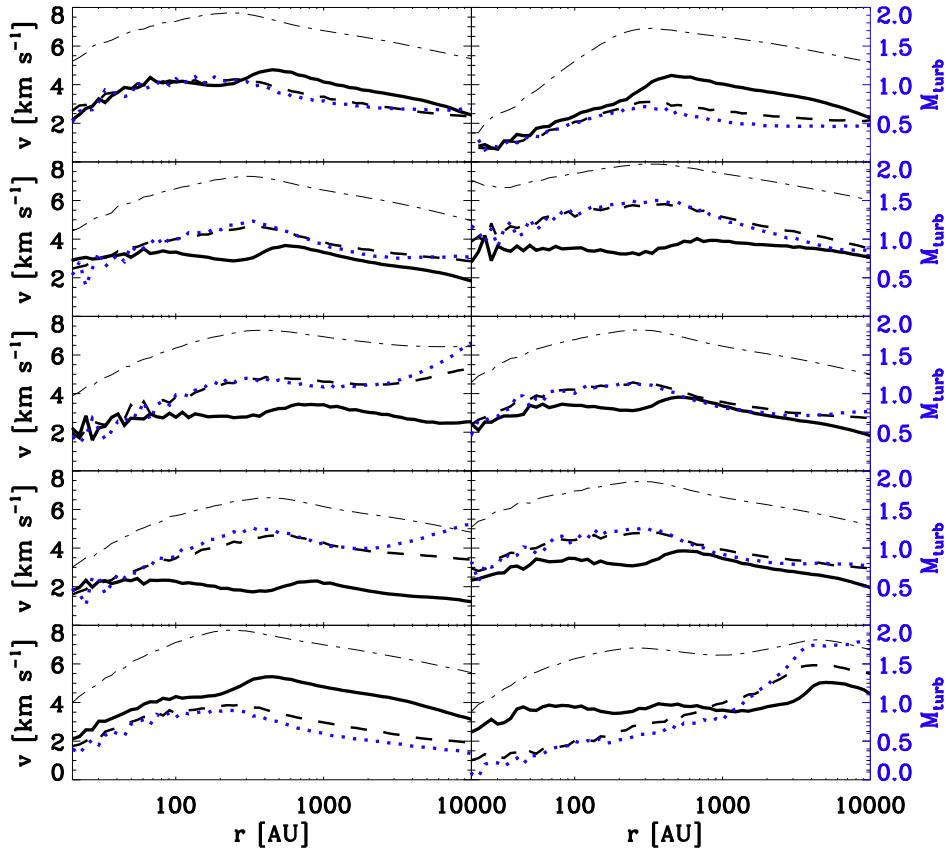
Figure 2. Velocity structure of the gas just prior to the formation of the first sink particle in each minihalo. Minihaloes are shown in order going from top left to bottom right. Solid lines show radial velocity $v_{\rm rad}$, dashed lines depict rotational velocity $v_{\rm rot}$, and dash-dot lines show the free-fall velocity $v_{\rm ff}$. Blue dotted lines represent $M_{\rm turb}$ and follow the scaling shown on the right-hand y-axis. Turbulence is generally sonic ($M_{\rm turb}$=1), though in some cases the level of turbulence can become mildly supersonic. Over these distance scales, $v_{\rm rad}$ and $v_{\rm rot}$ both remain on the order of $\sim 1/2$ of $v_{\rm ff}$. While the H$_2$ chemistry leads to very similar thermal histories for each minihalo, differences in mass inflow history yield a greater variety in the velocity structure of the inner gas. In particular, the relative magnitude of $v_{\rm rad}$ and $v_{\rm rot}$ differs in each case. Though they remain within a factor of two of each other, $v_{\rm rad}$ dominates in some cases while $v_{\rm rot}$ dominates in others.

and neighboring haloes can be safely ignored. Also note that the gas at the cut-out edge has a free-fall time of $\sim 10^7$ yr and will undergo little evolution over the next 5000 yr followed in the simulation. Our cut-out technique leads to the propagation of a rarefaction wave starting from the cut-out edge due to the vacuum boundary condition. However, the wave will only travel a distance of $c_s t$, where c_s is the gas sound-speed (~ 2 km s^{-1}), and the time t is 5000 yr. This corresponds to an insignificant distance of $\sim 10^{-2}$ pc (2000 AU) from the cut-out edge, over two orders of magnitude smaller than the 10 pc box size.

In addition, each remaining SPH particle is replaced with 256 child particles, each of which is placed randomly within the smoothing kernel of the parent particle. The mass of the parent particle is then evenly divided amongst the child particles. Each of these particles inherits the same chemical abundances, velocity, and entropy as the parent particle (see, e.g., Bromm & Loeb 2003; Clark et al. 2011b).

This ensures conservation of mass, internal energy, and linear momentum. After this process, each SPH particle in the new cut-out simulation has a mass of $m_{\rm sph} = 7.2 \times 10^{-3}$ M$_\odot$, and the new resolution mass is $M_{\rm res} \simeq 0.4$ M$_\odot$, the approximate mass contained in one SPH kernel (Bate et al. 1995). The cut-out and refinement is performed for the central star-forming region within each of the ten identified minihaloes. We then evolve the star-forming disks in these ten different minihaloes over 5000 yr of protostellar accretion.

2.3   Chemistry, Heating, and Cooling

We utilize the same chemistry and thermal network as described in detail by Greif et al. (2009) and used in Stacy et al. (2012). Briefly, the code follows the abundance evolution of H, H$^+$, H$^-$, H$_2$, H$_2^+$, He, He$^+$, He^{++}, and e$^-$, as well as the three deuterium species D, D$^+$, and HD. All relevant cooling mechanisms, including H$_2$ collisions with H
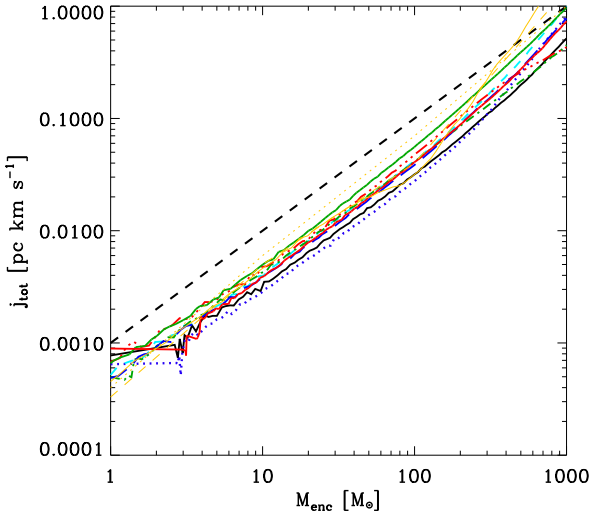
Figure 3. Angular momentum profile of gas within each mini-halo, measured just prior to the formation of the first sink. The thick lines of various colors and linestyles represent eight different minihaloes from our suite. The thin yellow lines denote angular momentum profiles found in separate cosmological simulations. Solid yellow line is taken from Stacy et al. (2010), dotted yellow line from Yoshida et al. (2006), and dashed yellow line from Abel et al. (2002). Thick black dashed line shows an approximate powerlaw fit to these profiles, $j \propto M_{enc}$ Note the near convergence of each of these angular momentum profiles, including profiles obtained from varying cosmological realizations and differing techniques for hydrodynamics computation.

and He as well as other H_2 molecules, are included. The thermal network also includes cooling through H_2 collisions with protons and electrons, H and He collisional excitation and ionization, recombination, bremsstrahlung, and inverse Compton scattering off the cosmic microwave background.

Further H_2 processes are also included to properly model gas evolution to high densities. For instance, the chemistry and thermal network includes three-body H_2 formation and the concomitant H_2 formation heating, which become important at $n \gtrsim 10^8$ cm^{-3}. Three-body H_2 formation rates are uncertain, however, and Turk et al. (2011) determined that the variation in suggested rates leads to significant differences in the gas collapse at high density, including long-term disk stability and fragmentation. For our simulations, we choose the intermediate rate from Palla et al. (1983). When $n \gtrsim 10^9$ cm^{-3}, cooling through H_2 rovibrational lines becomes less effective as these lines grow optically thick. We account for this using an escape probability formalism together with the Sobolev approximation (see Yoshida et al. 2006; Greif et al. 2011 for further details).

2.4 Sink Particle Method

SPH particles that reach densities of $n_{max} = 10^{13}$ cm^{-3} are converted into sink particles. Sinks grow in mass by accreting surrounding gas particles that lie within a distance of r_{acc}, where $r_{acc} = L_{res} \simeq 20$ AU, and

$$L_{res} \simeq 0.5 \left(\frac{M_{res}}{\rho_{max}} \right)^{1/3}. \tag{1}$$

Along with the criterion that the accreted particles must be within a distance $d < r_{acc}$ from the sink, we also require that the particles are not rotationally supported against infall onto the sink. This corresponds to $j_{SPH} < j_{cent}$, where $j_{SPH} = v_{rot}d$ is the specific angular momentum of the gas particle, $j_{cent} = \sqrt{GM_{sink}r_{acc}}$ is the angular momentum required for centrifugal support, and v_{rot} and d are the rotational velocity and distance of the particle relative to the sink. In addition, a sink accretes all particles which come within $d < r_{min} = 4$ AU. These same criteria are used not only for gas particles but also neighboring sink particles, so our algorithm allows for the merging of two sink particles. When the sink first forms, it immediately accretes the majority of particles within r_{acc}, giving it an initial mass of $M_{res} \simeq 0.4$ M$_\odot$. Each time the sink grows, its position and velocity are set to the mass-weighted of that of the sink and the accreted particles.

After a particle becomes a sink, its density, temperature, and chemical abundances are no longer updated, though its position and velocity continue to evolve through gravitational interactions. Each sink is instead held at a constant density n_{max} and temperature of 1000 K. The sink thus exerts a pressure on the surrounding particles, avoiding the formation of an artificial pressure vacuum around its accretion radius (see Bromm et al. 2002; Martel et al. 2006).

Once a sink is formed, nearly all gas particles near the sinks will be accreted before approaching the $d < r_{min}$ criterion. However, secondary sinks can come within this distance and become subject to strong N-body interactions. In physical reality, however, the sub-sink region will contain not only the protostar but also surrounding gas and an accretion disk. In addition, the protostars themselves can be very distended, with photospheres reaching ~ 1 AU (e.g. Omukai & Palla 2003; Greif et al. 2012; Smith et al. 2012a). Our accretion of all secondary sinks within $d < r_{min}$ therefore allows us to account for sub-sink hydrodynamic affects which will mitigate those of pure N-body dynamics.

2.5 Identifying Binaries

Once a protostellar multiple system has formed, we identify which pairs of sinks comprise a binary system. For each minihalo we determine which pairs of sinks are gravitationally bound by comparing their specific potential and kinetic energies, ϵ_p and ϵ_k. A pair of sinks is considered a binary system if $\epsilon < 0$, where ϵ is the total orbital energy,

$$\epsilon = \epsilon_p + \epsilon_k, \tag{2}$$

$$\epsilon_p = \frac{-G(M_1 + M_2)}{r}, \tag{3}$$

and

$$\epsilon_k = \frac{1}{2}v^2. \tag{4}$$

M_1 and M_2 are the masses of the two sinks in question, r is the distance between the sinks, and v is the relative velocity between the sinks. Within each minihalo we find an average of between two and three binaries.

Each binary is then assigned an overall mass $M_{bin} = M_1 + M_2$, a center-of-mass position, and a center-of-mass velocity. We next determine the semi-major axis, a, for each
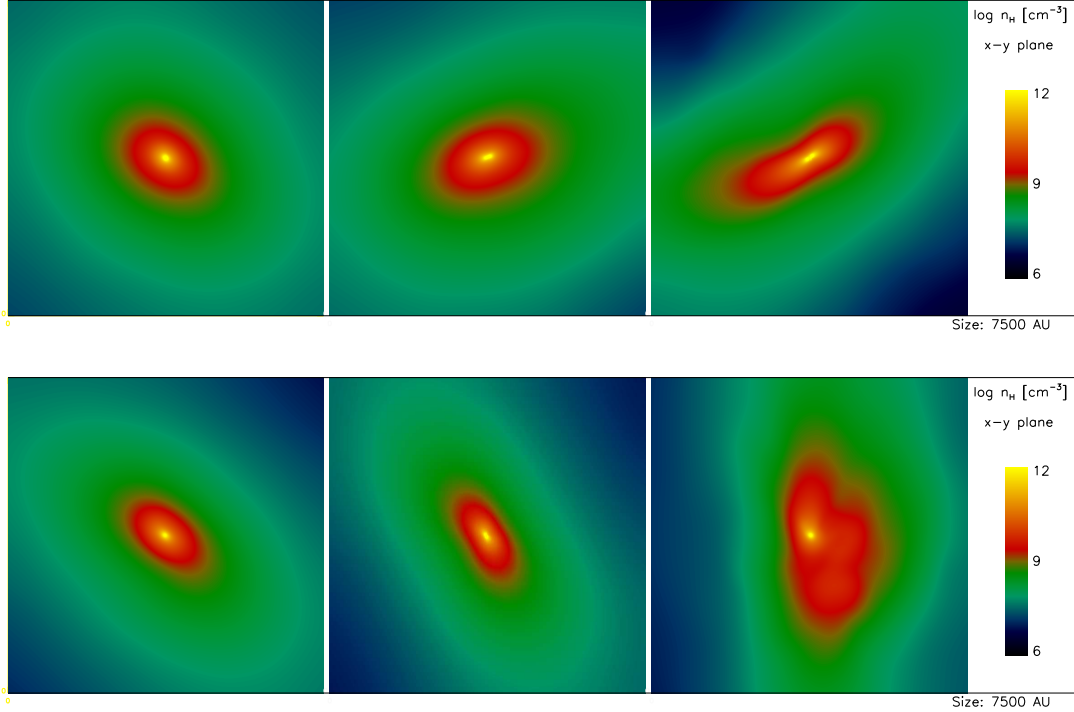
Figure 4. Density structure of the gas just prior to the formation of the first sink particle in six select minihaloes. Each star-forming region has a similar structure which roughly follows that of an isothermal sphere. However, the gas within differing minihaloes does vary somewhat in the degree of flattening.

binary. This is derived by equating the above definition of ϵ with the following energy equation:

$$\epsilon = \frac{-GM_{\rm bin}}{2a}. \tag{5}$$

This yields

$$a = \frac{-G\,(M_1 + M_2)}{2\,(\epsilon_{\rm k} + \epsilon_{\rm p})}. \tag{6}$$

We furthermore calculate the binary's mass ratio q, where

$$q = \frac{M_2}{M_1}. \tag{7}$$

In this case M_2 corresponds specifically to the less massive of the binary members, and M_1 corresponds to the more massive, such that the value of q is always between zero and one.

3   RESULTS

3.1   Initial Minihalo Collapse

The initial collapse of gas to protostellar density exhibits substantial similarity within each minihalo. Figure 1 shows the thermal state of the star-forming gas within each minihalo just prior to the formation of the first high-resolution sink, while Figure 2 shows their velocity profiles. At high densities of $n > 10^8$ cm^{-3}, H$_2$ three-body formation becomes rapid. This leads to nearly isothermal evolution as increased H$_2$ cooling counteracts adiabatic heating while the gas condenses to $n > 10^{12}$ cm^{-3}. The minihaloes show a striking

similarity in thermal evolution in this density range. In the evolution of gas to the densities shown in Figure 1 ($n > 10^6$ cm^{-3}), we also find that the HD cooling is generally unimportant compared to H$_2$ cooling,

Figure 3 shows the angular momentum profile of the gas in the maximally resolved simulations just before the first sink has formed, measured with respect to the center-of-mass of all gas included in the 10 pc simulations. These profiles all have roughly the same magnitude and powerlaw slope, such that $j(r) \propto M_{\rm enc}$, where $M_{\rm enc}$ is the enclosed gas mass within a given radius r from the center-of-mass. This convergence is found not only among minihaloes in our simulation, but also including those from differing cosmological realizations, performed with varying methods of computational hydrodynamics (Abel et al. 2002; Yoshida et al. 2006). These angular momentum distributions may additionally lead to high spin rates of individual protostars (e.g. Stacy et al. 2011, 2012).

The density structure of the central gas can be seen in Figure 4 for a representative number of the minihaloes. The similarity between minihaloes is again apparent, though some of the star-forming gas exhibits greater elongation and a more disk-like structure. Similar variation is seen when we compare the velocity and turbulent structure in Fig. 2. We measure $M_{\rm turb}$ over a range of radial bins according to the following:

$$M_{\rm turb}^2 c_s^2 = \sum_i \frac{m_i}{M} \left(v_i - v_{\rm rot} - v_{\rm rad}\right)^2, \tag{8}$$

where c_s is the sound speed of the radial bin, m_i is the mass of a gas particle contributing to the bin, and M is the total
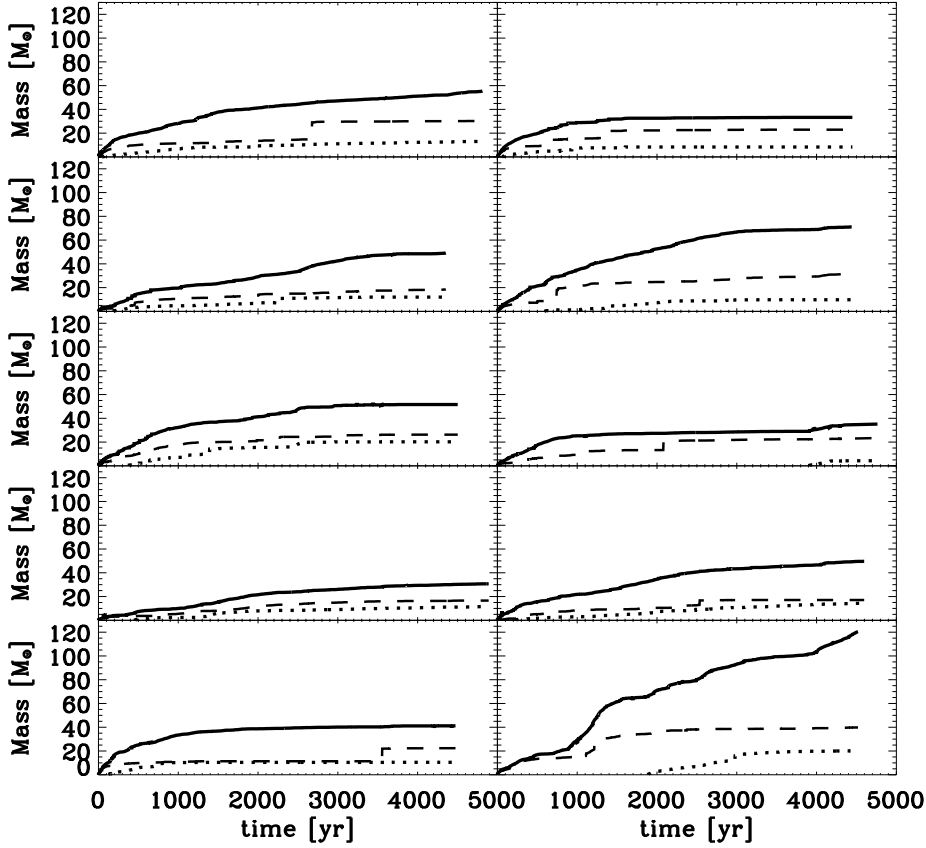
Figure 5. History of the mass growth of the stellar systems in each minihalo. Solid lines represent the total sink mass. Dashed lines show the growth of the most massive sink. Dotted lines depict the growth of the second-most massive sink. Average accretion rates vary by over a factor of three between minihaloes.

mass of the bin. Between 20 and 10,000 AU, both the rotational velocity $v_{\rm rot}$ and radial velocity $v_{\rm rad}$ remain at a few km s^{-1}, while the turbulence remains approximately sonic, never reaching more than twice the thermal velocity of the gas. In each case, both radial and infall velocities are on the order of $\sim 1/2$ of the free-fall velocity $v_{\rm ff}$. However, the relative magnitude of $v_{\rm rad}$ and $v_{\rm rot}$ varies, with $v_{\rm rad}$ dominating in some cases and $v_{\rm rot}$ dominating in others.

After the central gas in each minihalo reaches the density threshold for sink formation, in all cases a stellar multiple system quickly forms. This fragmentation is in agreement with the parameter study of Machida et al. (2008). They modeled their initial conditions as modified Bonnor-Ebert spheres, which well-describes collapsing and approximately isothermal gas like that within star-forming regions (e.g. Ebert 1955; Bonnor 1956; Stacy et al. 2010; Greif et al. 2012), and found the following fragmentation condition:

$$\Omega_0 > \Omega_{\rm crit} = 4 \times 10^{-17} \left(\frac{n_0}{10^3 {\rm cm}^{-3}} \right)^{2/3} {\rm s}^{-1}, \qquad (9)$$

where Ω_0 and n_0 are the angular velocity and central number density of the initial core of the Bonnor-Ebert sphere. We determine Ω_0 of the central core when n_0 is between

10^3 cm^{-3} and 10^4 cm^{-3}, corresponding to $\Omega_{\rm crit}$ values between $\gtrsim 4 \times 10^{-17}$ s^{-1} and $\sim 2 \times 10^{-16}$ s^{-1}. We take a mass-weighted average of the angular velocity of all gas particles with $n > 10^3$ cm^{-3} and find in each case that Ω_0 ranges between two to three orders of magnitude greater than $\Omega_{\rm crit}$. The subsequent flattening and fragmentation of the dense gas is thus consistent with the criterion presented by Machida et al. (2008).

3.2 Mass Function

The mass growth history of the sinks shows substantial variation among the ten minihaloes, as is shown in Figures 5 and 6. At the end of the simulations, the total mass accreted by all sinks ranges from $30 - 120\,{\rm M_\odot}$ for a given minihalo (Fig. 5). The total mass of gas within each minihalo is typically $\lesssim 10^5$ M$_\odot$, implying a star-formation efficiency of $\sim 10^{-3}$. The distribution of sink masses after 5000 yr of accretion can be seen for the individual minihaloes in Figure 6, where the variation between minihaloes is even more striking. In particular, while some minihaloes have only one or two sinks with $M_* < 1$ M$_\odot$, this number can be as large as nine. We
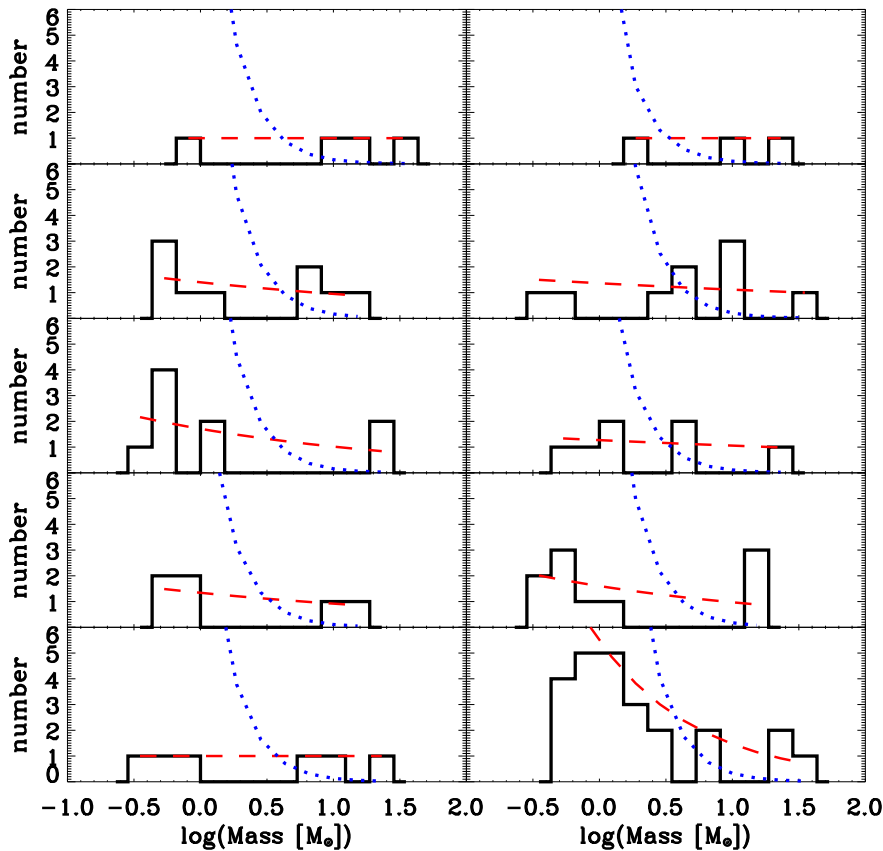
Figure 6. Distribution of sink masses in each minihalo after ~ 5000 yr of accretion. Dashed red lines depict powerlaw fits to each distribution, $dN/dm \propto M_*^{-\alpha}$. We find that α ranges from zero (Minihaloes 1 and 2) to 0.57 (Minihalo 10). Dashed blue lines show an example distribution for $\alpha = 2$, the minimum powerlaw that will yield a top-heavy mass function. Each $\alpha = 2$ distribution is normalized to have the same total mass as that found within the sinks of the corresponding minihalo.

find a range of powerlaw fits to the relation $dN/dm \propto M_*^{-\alpha}$, where N is the number of sinks that lie within a logarithmically scaled mass bin. This range extends from $\alpha = 0$ for Minihaloes 1, 2 and 9, to $\alpha = 0.57$ for Minihalo 10. Considering the distribution across all minihaloes (Fig. 7), we find $dN/dm \propto M_*^{-0.17}$.

Unlike the observed present-day initial mass function (IMF), which is characterized by a Salpeter slope of $\alpha = 2.35$ towards the high mass end, our simulations yield a top-heavy mass function in that the majority of the protostellar mass resides within the most massive protostars. Top-heaviness applies to mass functions with $\alpha < 2$, since this is the requirement for the average stellar mass to be dominated by the upper limit of the mass range (e.g. Bromm 2012). If we consider smaller values of α to be more top-heavy, then our fitted mass function is less top-heavy than that found after ~ 1000 yr of sink accretion in Greif et al. (2011), who find $\alpha \lesssim 0$.

Including radiative feedback would likely modify our values for α, though the magnitude of the modification is uncertain. While feedback does not prevent fragmentation (e.g. Smith et al. 2011, Stacy et al. 2012b), heating of the

gas may suppress low-mass fragmentation to yield smaller α values closer to zero (i.e., a flatter spectrum). Greif et al. (2011) resolved smaller mass scales and again found smaller values of α. However, following such a resolved simulation for longer than their 1000 yr may reveal a population of very low-mass stars that arises at later times, instead increasing α. Our simulations do not resolve down to the opacity limit of fragmentation, the scale on which a small $\sim 10^{-2}$ $M_\odot$ hydrostatic core first forms (e.g. Rees 1976; Omukai & Nishi 1998; Greif et al. 2012). We may therefore underestimate the number of such low-mass protostellar fragments that form.

3.3 Binary Fraction and Merger Rate

Every minihalo contains at least one binary, and on average each halo hosts between two and three binaries. We define the binary fraction as

$$f_B = \frac{B}{S + B}, \tag{10}$$

where S and B are the number of single and binary systems, respectively. Summing over all sinks remaining in each
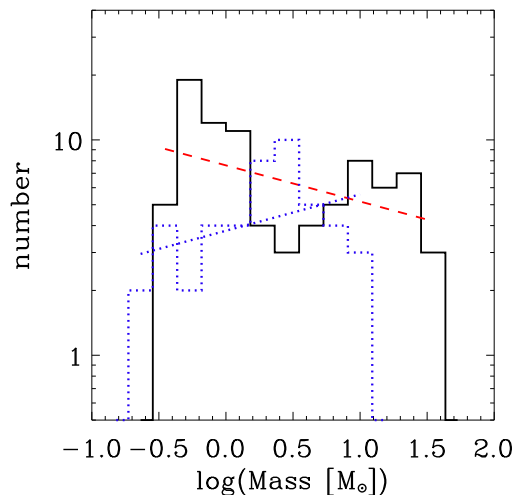
lation is significantly steeper. As will further be discussed in Section 4, there are multiple reasons for this. The spatial resolution of the simulations was limited, so the distributions cannot sample orbits with $a < 20$ AU. This contributes to the apparent lack of hard binaries. In addition, the binaries have only evolved for a few thousand years, and their orbits may evolve and harden over longer periods of time.

The distribution of mass ratio q (Figure 9) goes as $dN/dq \propto q^{-0.55}$, while for the cumulative distribution we find a best-fit powerlaw of $F_q \propto q^{0.75}$. The average value of q is 0.35. We compare our q distribution to that found for solar-type stars by Duquennoy & Mayor (1991), shown as the blue dotted line in Fig. 9. They observed a q-distribution peaked at 0.23, while our distribution is peaked at $q < 0.1$, so our simulations have a comparatively high fraction of low-q binaries.

Our rate of low-q binaries is also high when compared with more massive star clusters in the Milky Way. For instance, Kiminki & Kobulnicky (2012) find that $dN/dq \propto q^{0.1}$, while our fit falls off much more steeply and is slightly outside their range of error. Sana & Evans (2011) present observations which yield a uniform distribution of q down to $q = 0.2$. This corresponds to the cumulative distribution shown as the blue line in the right panel of Fig. 9.

If the sink particles of the simulations continued to accrete mass for longer periods of time, it is possible that the q distribution would shift toward a larger percentage of binaries with nearly equal mass. As described in, e.g., Bate & Bonnell (1997), if gas with sufficient angular momentum flows onto a binary star, it will accrete preferentially onto the less massive companion. Angular momentum conservation prevents rotating gas from reaching the larger star without the aid of, e.g., gravitational torques. The gas instead remains at some radius beyond the more massive star where it is more easily captured by the less massive companion, resulting in a tendency for q to evolve towards a value of one. This is similar to the fragmentation-induced starvation described by Peters et al. (2010). In their simulations of star-forming molecular clouds, they found that gas inflowing through a stellar disk was accreted by lower-mass stars before it could reach the more massive and centrally-located star.

Figure 7. Total distribution of sink masses in all minihaloes. Red dashed line depicts a powerlaw fit to the overall distribution, $dN/dm \propto M_*^{-0.17}$. Blue dotted lines depict the total mass distribution from the 'merging sink' simulations of Greif et al. 2011 and a powerlow fit to this distribution ($\alpha = -0.17$).

minihalo at the end of the simulations, we have $S = 42$ and $B = 24$, yielding $f_B = 0.36$. Calculated slightly differently, this means any individual star has a probability $2B/(S + 2B) = 53\%$ of having a binary companion. This is a substantial fraction, and similar to the range of massive star binary fractions observed in various clusters in the Milky Way (e.g. Sana & Evans 2011; Kiminki & Kobulnicky 2012).

While a total of 217 sinks form in our suite of minihaloes, 90 remain after 5000 yr. Over than half (59%) of the sinks are therefore lost to mergers. This is similar to the merger rate found in Greif et al. (2012). However, it will require higher-resolution simulations to determine which of these mergers were actually unresolved but long-lived tight ($a < 20$ AU) binaries. The results of Greif et al. (2012), as well as our criterion that only non-rotationally supported sinks are merged, support the likelihood that a large number of these sink mergers were indeed true protostellar mergers.

3.4 Orbital Period and Mass Ratio Distribution

The characteristics of the binary distribution are shown in Figures 8 and 9. The distribution of the binary periods is peaked at $10^{5.5}$ days, or 870 yr. In comparison with nearby solar-type stars (blue dotted line in Fig. 8), this peak is shifted to longer periods. For instance, (Duquennoy & Mayor 1991) observed a P distribution that is peaked at $10^{4.8}$ days, or 170 years. This corresponds to a distribution of the semi-major axis, a, that is peaked around ~ 250 AU, with an average value of 760 AU. In Figure 8 we also show the related cumulative distribution of the binary periods, F_P, normalized such that $F_P(P < \infty) = 1$. We display a best-fit power-law for this distribution, $F_P \propto \log(P)^{2.54}$, and compare to a 'Öpik distribution' (Öpik 1925), where $F_P \propto \log(P)$. Öpik's law is consistent with observations of massive star binaries (e.g. Kouwenhoven et al. 2007; Sana & Evans 2011; Kiminki & Kobulnicky 2012). However, the fit found from our simu-

3.5 Protostellar Ejection Rate

Of the total of 90 sinks remaining at the end of our simulation, 39 have radial velocities that are greater than their escape velocities (Figure 10), where we define $v_{\rm esc}$ as

$$v_{\rm esc} = \sqrt{\frac{GM_{\rm enc}}{r}}, \tag{11}$$

where $M_{\rm enc}$ is the mass enclosed between the center of mass (COM) and the sink particle at distance r from the COM. The COM is determined using all gas and sink particles with $n > 10^{10}$ cm^{-3}. Roughly half (43%) of the sinks can thus leave the stellar disk, similar to the rate found in, e.g. Greif et al. (2011) in their simulations of primordial star formation and Bate et al. (2003) in their numerical studies of present-day, low-mass star formation.

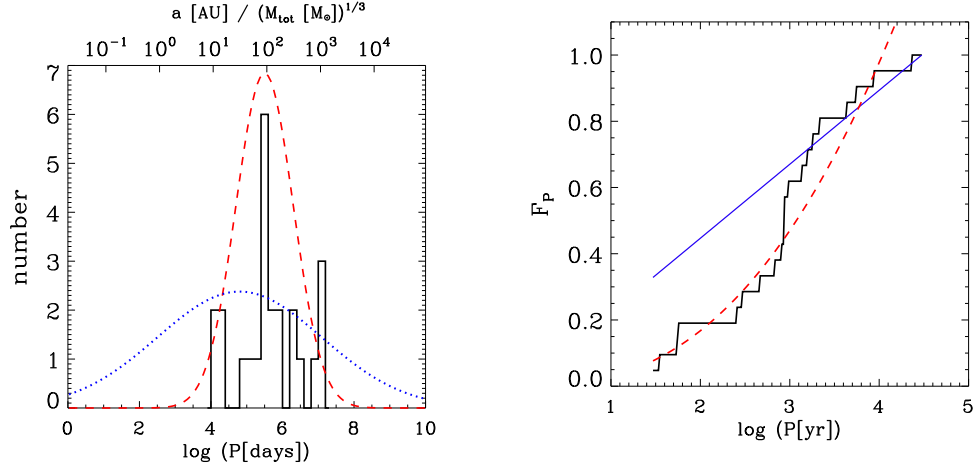In addition, we define a second escape velocity, that required to exit the minihalo:

Figure 8. *Left:* Distribution of the log of the period, P, for the binaries found within each minihalo. Note that units of P is in days. Red dashed line shows a Gaussian fit to the distribution. Blue dotted line shows an example fit to data for solar-type stars (Duquennoy & Mayor 1991). The distribution of the binary periods is peaked at $10^{5.5}$ days, or 870 yr. *Right:* Cumulative distribution F_P of the orbital period of the binaries identified in all minihaloes. Red dashed line shows a powerlaw fit, $F_P \propto \log(P)^{2.54}$, while the blue line shows a sample Öpik distribution for comparison.
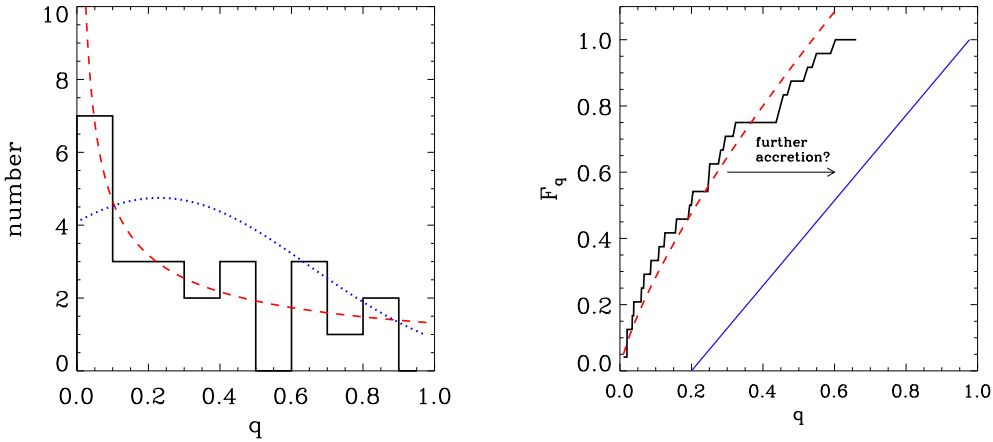

Figure 9. *Left:* Distribution of the mass ratio q between the members of binaries located in each minihalo. Red line is the powerlaw fit $dN/dq \propto q^{-0.55}$. Blue dotted line shows an example fit to data for solar-type stars (Duquennoy & Mayor 1991). The average value of q is 0.34. *Right:* Cumulative distribution F_q of the mass ratio of all binaries in our simulation. Red dashed line is a powerlaw fit, $F_q \propto q^{0.75}$. The blue line depicts a uniform distribution down to $q = 0.2$, as observed in massive star clusters in the Milky Way (e.g. Sana & Evans 2011).

$$v_{esc,halo} = \sqrt{\frac{GM_{halo}}{r_{halo}}} \sim 5\,\mathrm{km\,s^{-1}}, \qquad (12)$$

where we define $M_{halo} = 4 \times 10^5$ $M_\odot$ and $r_{halo} = 80$ pc, the average values for the minihaloes of our suite. Whether v_{esc} or $v_{esc,halo}$ is larger varies depending on the sink and its location. A total of 53 sinks have $v_{rad} > v_{esc,halo}$, which is greater than the 39 which can escape from the stellar disk. Thus, the gravity of the stellar disk provides the stronger escape condition. In the majority of cases, for a sink to have sufficient velocity to escape the disk, it must already have sufficient velocity to escape the minihalo (left panel of Figure 10). For a sink traveling at $v_{esc,halo}$, the time to cross the virial radius of the minihalo is $\sim 2 \times 10^7$ yr. Note that

within this time the minihalo is not expected to undergo significant mass growth itself, no more than doubling in mass (e.g. Stacy et al. 2011b, Wechsler et al. 2002). Thus, $v_{esc,halo}$ will not increase by more than 1-2 km s^{-1}.

Of the ejected protostars, 18 are of mass $M_* < 1$ $M_\odot$ and thus have a possibility of surviving to the present day (Clark et al 2011b). This depends, however, on whether the stars will accrete more mass at a later time and thus become shorter lived. Identifying them as Pop III stars would require that, as they become incorporated into the Milky Way or nearby dwarf galaxies, they will not accrete any enriched material that will remain in their atmospheres and mask them as Pop II stars (e.g. Frebel et al. 2009; Johnson & Khochfar 2011).
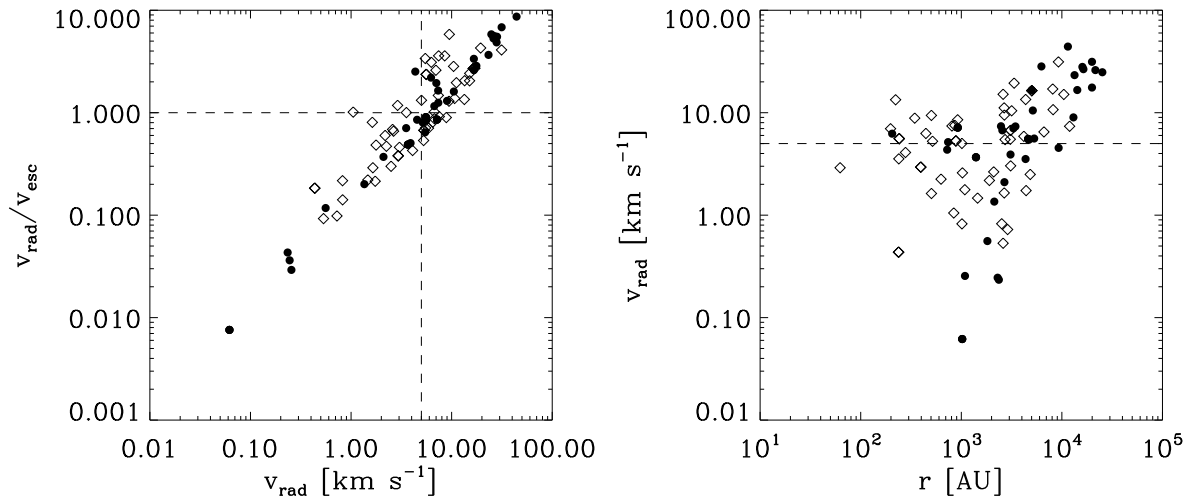
Figure 10. *Left:* Ratio of $|v_{\rm rad}|$ to $v_{\rm esc}$ for each sink particle. Sinks with $M_* < 1\,{\rm M}_\odot$ are denoted with filled circles, while diamonds represent sinks with $M_* > 1\,{\rm M}_\odot$. Horizontal dashed line shows where $|v_{\rm rad}/v_{\rm esc}| = 1$. Sinks above the horizontal dashed line are able to escape from the stellar disk. The vertical dashed line denotes $v_{\rm esc,halo}$, the velocity necessary to escape the minihalo. *Right:* Variation of $|v_{\rm rad}|$ with radius. Dashed line again shows $v_{\rm esc,halo}$.

4   CAVEATS

The results presented in the simulation have a number of caveats that should be noted. First, these simulations followed only 5000 yr of protostellar mass accretion. The distribution of sink masses and binary properties will continue to evolve beyond this point, as some of the sinks will continue to grow in mass and orbits may harden or undergo disruption through close encounters with other sinks. We also cannot study binaries within the resolution limit of the simulation, 20 AU. Thus, the sink mergers discussed previously may have instead become very tight and unresolved binaries. Objects formed from subsequent fragmentation on sub-sink scales also could not be addressed in this study. If we did presume that all sink mergers instead became tight binaries orbiting with semi-major axis of 10 AU, we would have a binary fraction of 73%. The average orbital radius of all binaries would then be 170 AU, and the average mass ratio would still be 0.34.

   In addition, we do not include protostellar feedback in our simulations. The H_2-dissociating and ionizing radiation emitted from the growing protostars may substantially change the characteristics of the stellar disk and eventually cut off mass flow onto the disk altogether (e.g. Hosokawa et al. 2011; Smith et al. 2011; Stacy et al. 2012b). Another important physical process not included in our simulations was magnetic fields, which may affect the angular momentum build-up of the protostellar disk, the subsequent fragmentation, and the mass flow onto the protostars (e.g. Tan & Blackman 2004; Silk & Langer 2006; Maki & Susa 2007; Schleicher et al. 2010; Federrath et al. 2011; Sur et al. 2012; Schober et al. 2012a, 2012b). In the future we plan to enhance the physical realism of subseqent simulations by including these processes and resolving smaller scales.

5   SUMMARY AND CONCLUSIONS

We have examined the formation of Pop III multiple systems within ten different minihaloes extracted from a 1.4 Mpc (comoving) cosmological box. The properties of each stellar group varies between minihaloes, with mass functions ranging from flat to $\alpha = 0.57$, and average stellar accretion rates varying by over a factor of three between minihaloes.

   Looking at the combined properties of the ten stellar systems, we find that 50% of the protostars merge with larger protostars, while 50% of the remaining protostars are ejected from their stellar disk. We furthermore find a binary fraction of $\sim 36\%$, translating to a 53% probability that any given star will have a companion. Some of these binaries have semi-major axes that extend to 3000 AU. The distribution of semi-major axes peaks slightly at ~ 300 AU, while the mass ratio is nearly uniformly distributed between zero and one. Recent work by Smith et al. (2012b) implies that this result may be modified by the effects of heating and ionization from DM annihilation (DMA). If their findings hold up to further investigation, DMA may suppress fragmentation and lead to wider binaries of $a > 1000$ AU.

   Our simulation did not have sufficient resolution to resolve protostellar mergers or the formation of tight binaries, as these processes occur on scales smaller than our resolution length of 20 AU. If a significant fraction of these sink mergers did represent true protostellar mergers or the formation of contact binaries, this has important implications for the Pop III stellar evolution (see, e.g. Langer 2012 and references therein). During a common-envelope phase, H-envelope removal by a close binary companion may allow for a star as low as 10 ${\rm M}_\odot$ to become a WR star (e.g. Vanbeveren et al. 1998; Crowther 2007). A stellar merger may rejuvenate the mass-gaining star, making it appear younger than its true age (e.g. Hellings 1983; Braun & Langer 1995; Dray & Tout 2007). Alternatively, a star with an undermassive helium core may result (Braun & Langer 1995). Such stars

may avoid the red supergiant phase and instead explode as blue supergiants. Mass accretion through Roche-lobe overflow may also spin up a star, allowing for rotationally-induced mixing and possibly chemically homogeneous evolution, thereby altering the star's luminosity, temperature, and metal production (e.g. Ekström et al. 2008; Yoon et al. 2012). In particular, rotationally induced mixing may alter the nucleosynthesis within a within a low-metallicity or primordial massive star to yield greater CNO-element abundances, especially ^{14}N (e.g. Ekström et al. 2008; Yoon et al. 2012). This additionally leads to a neutron excess in the core, enhancing the production of s-process elements (e.g. Pignatari et al. 2008).

The binarity of Pop III stars also provides an important pathway for the formation of GRBs and high-mass X-ray binaries. If one of the binary members is in the mass range to collapse into a BH, then a close companion may remove its hydrogen envelope and allow for penetration of a GRB jet to the surface (e.g. Lee et al. 2002; Izzard et al. 2004). Once the BH remnant is left behind, the Roche lobe overflow from the companion enables the BH to sustain a high luminosity and X-ray flux. These sources could significantly contribute to reionization, and exert feedback effects during the assembly of the first galaxies (Mirabel et al. 2011; Jeon et al. 2012).

Pop III binarity is thus a crucial aspect to understanding Pop III evolution and feedback. A significant percentage of Pop III stars exist in binaries and undergo stellar mergers. Greater computational power will allow for future simulations which include more physical processes such as feedback and magnetic field growth, and which will also follow the evolution of Pop III multiple systems with increased resolution over longer periods of time. Combined with observational constraints, this will yield an increasingly refined understanding of Pop III stars and their role in the early Universe.

REFERENCES

Abel T., Bryan G. L., Norman M. L., 2002, Sci, 295, 93
Alvarez M. A., Bromm V., Shapiro P. R., 2006, ApJ, 639, 621
Alvarez M. A., Wise J. H., Abel T., 2009, ApJ, 701, L133
Bate M. R., Bonnell I. A., 1997, MNRAS, 285, 33
Bate M. R., Bonnell I. A., Bromm V., 2003, MNRAS, 339, 577
Bate M. R., Bonnell I. A., Price N. M., 1995, MNRAS, 277, 362
Bonnor W. B., 1956, MNRAS, 116, 351
Braun H., Langer N., 1995, A&A, 297, 483
Bromm V., 2012, Second Workshop on Numerical and Observational Astrophysics: From the First Structures to the Universe Today (arXiv: 1203.3824)
Bromm V., Coppi P. S., Larson R. B., 2002, ApJ, 564, 23
Bromm V., Kudritzki R. P., Loeb A., 2001, ApJ, 552, 464
Bromm V., Loeb A., 2003, ApJ, 596, 34
Bromm V., Loeb A., 2004, New Astron., 9, 353
Bromm V., Yoshida N., Hernquist L., 2003, ApJ, 596, L135
Brott I., de Mink S. E., Cantiello M., Langer N., de Koter A., Evans C. J., Hunter I., Trundle C., Vink J. S., 2011, A&A, 530, A115
Cantiello M., Yoon S.-C., Langer N., Livio M., 2007, A&A, 465, L29
Chatzopoulos E., Wheeler J. C., 2012, ApJ, 748, 42
Clark P. C., Glover S. C. O., Klessen R. S., 2008, ApJ, 672, 757
Clark P. C., Glover S. C. O., Klessen R. S., Bromm V., 2011a, ApJ, 727, 110
Clark P. C., Glover S. C. O., Smith R. J., Greif T. H., Klessen R. S., Bromm V., 2011b, Sci, 331, 1040
Crowther P. A., 2007, ARA&A, 45, 177
de Mink S. E., Cantiello M., Langer N., Pols O. R., Brott I., Yoon S.-C., 2009, A&A, 497, 243
Donati J.-F., Landstreet J. D., 2009, ARA&A, 47, 333
Dray L. M., Tout C. A., 2007, MNRAS, 376, 61
Duquennoy A., Mayor M., 1991, A&A, 248, 485
Ebert R., 1955, Zeitschrift fr Astrophysik, 36, 222
Ekström S., Meynet G., Chiappini C., Hirschi R., Maeder A., 2008, A&A, 489, 685
Federrath C., Chabrier G., Schober J., Banerjee R., Klessen R. S., Schleicher D. R. G., 2011, Physical Review Letters, 107, 114504
Ferrario L., Pringle J. E., Tout C. A., Wickramasinghe D. T., 2009, MNRAS, 400, L71
Frebel A., Johnson J. L., Bromm V., 2009, MNRAS, 392, L50
Greif T., Springel V., White S., Glover S., Clark P., Smith R., Klessen R., Bromm V., 2011, ApJ, 737, 75
Greif T. H., Bromm V., Clark P. C., Glover S. C. O., Smith R. J., Klessen R. S., Yoshida N., Springel V., 2012, MNRAS, 424, 399
Greif T. H., Glover S. C. O., Bromm V., Klessen R. S., 2010, ApJ, 716, 510
Greif T. H., Johnson J. L., Bromm V., Klessen R. S., 2007, ApJ, 670, 1
Greif T. H., Johnson J. L., Klessen R. S., Bromm V., 2009, MNRAS, 399, 639
Haiman Z., 2011, Nat, 472, 47
Haiman Z., Thoul A. A., Loeb A., 1996, ApJ, 464, 523
Hamann W.-R., Gräfener G., Liermann A., 2006, A&A, 457, 1015
Heger A., Woosley S. E., 2002, ApJ, 567, 532
Hellings P., 1983, Ap&SS, 96, 37
Hosokawa T., Omukai K., Yoshida N., Yorke H. W., 2011, Science, 334, 1250
Izzard R. G., Ramirez-Ruiz E., Tout C. A., 2004, MNRAS, 348, 1215
Jeon M., Pawlik A. H., Greif T. H., Glover S. C. O., Bromm V., Milosavljević M., Klessen R. S., 2012, ApJ, 754, 34
Johnson J. L., Bromm V., 2007, MNRAS, 374, 1557

Johnson J. L., Greif T. H., Bromm V., 2007, ApJ, 665, 85

Johnson J. L., Khochfar S., 2011, MNRAS, 413, 1184

Karlsson T., Bromm V., Bland-Hawthorn J., 2012, Rev. Modern Phys., in press (arXiv: 1101.4024)

Kiminki D. C., Kobulnicky H. A., 2012, ApJ, 751, 4

Kitayama T., Yoshida N., Susa H., Umemura M., 2004, ApJ, 613, 631

Kouwenhoven M. B. N., Brown A. G. A., Portegies Zwart S. F., Kaper L., 2007, A&A, 474, 77

Kowalska I., Bulik T., Belczynski K., 2012, A&A, 541, A120

Kuhlen M., Madau P., 2005, MNRAS, 363, 1069

Langer N., 2012, ARA&A, 50, 107

Langer N., Cantiello M., Yoon S.-C., Hunter I., Brott I., Lennon D., de Mink S., Verheijdt M., 2008, in Bresolin F., Crowther P. A., Puls J., eds, IAU Symposium Vol. 250, Rotation and Massive Close Binary Evolution. p. 167

Lee C., Brown G. E., Wijers R. A. M. J., 2002, ApJ, 575, 996

Lee W. H., Ramirez-Ruiz E., 2006, ApJ, 641, 961

Linden T., Kalogera V., Sepinsky J. F., Prestwich A., Zezas A., Gallagher J. S., 2010, ApJ, 725, 1984

Machida M. N., Omukai K., Matsumoto T., Inutsuka S.-i., 2008, ApJ, 677, 813

Madau P., Ferrara A., Rees M. J., 2001, ApJ, 555, 92

Madau P., Rees M. J., Volonteri M., Haardt F., Oh S. P., 2004, ApJ, 604, 484

Maeder A., Meynet G., 2012, Rev. Modern Phys., 84, 25

Maio U., Khochfar S., Johnson J. L., Ciardi B., 2011, MNRAS, 414, 1145

Maki H., Susa H., 2007, PASJ, 59, 787

Martel H., Evans N. J., Shapiro P. R., 2006, ApJS, 163, 122

Mason B. D., Hartkopf W. I., Gies D. R., Henry T. J., Helsel J. W., 2009, AJ, 137, 3358

Meynet G., Maeder A., 2005, A&A, 429, 581

Milosavljević M., Bromm V., Couch S. M., Oh S. P., 2009, ApJ, 698, 766

Mirabel I. F., Dijkstra M., Laurent P., Loeb A., Pritchard J. R., 2011, A&A, 528, A149

Mori M., Ferrara A., Madau P., 2002, ApJ, 571, 40

Nakauchi D., Suwa Y., Sakamoto T., Kashiyama K., Nakamura T., 2012, ApJ, in press (arXiv: 1207.2835)

Norman M. L., O'Shea B. W., Paschos P., 2004, ApJ, 601, L115

Omukai K., Nishi R., 1998, ApJ, 508, 141

Omukai K., Palla F., 2003, ApJ, 589, 677

Öpik E., 1925, Tartu Obs. Publ., 26, 1

Palla F., Salpeter E. E., Stahler S. W., 1983, A[J, 271, 632

Peters T., Banerjee R., Klessen R. S., Mac Low M.-M., Galván-Madrid R., Keto E. R., 2010, ApJ, 711, 1017

Petrovic J., Langer N., van der Hucht K. A., 2005, A&A, 435, 1013

Petrovic J., Langer N., Yoon S.-C., Heger A., 2005b, A&A, 435, 247

Pignatari M., Gallino R., Meynet G., Hirschi R., Herwig F., Wiescher M., 2008, ApJ, 687, L95

Rees M. J., 1976, MNRAS, 176, 483

Ricotti M., Ostriker J. P., 2004, MNRAS, 352, 547

Sana H., de Mink S. E., de Koter A., Langer N., Evans C. J., Gieles M., Gosset E., Izzard R. G., Le Bouquin J.-B., Schneider F. R. N., 2012, Sci, 337, 444

Sana H., Evans C. J., 2011, in Neiner C., Wade G., Meynet G., Peters G., eds, IAU Symposium Vol. 272 of IAU Symposium, The multiplicity of massive stars. pp 474–485

Schaerer D., 2002, A&A, 382, 28

Schleicher D. R. G., Banerjee R., Sur S., Arshakian T. G., Klessen R. S., Beck R., Spaans M., 2010, A&A, accepted (arXiv: 1003.1135)

Schober J., Schleicher D., Federrath C., Glover S., Klessen R. S., Banerjee R., 2012a, ApJ, 754, 99

Schober J., Schleicher D., Federrath C., Klessen R., Banerjee R., 2012b, PRE, 85, 026303

Silk J., Langer M., 2006, MNRAS, 371, 444

Smith R. J., Glover S. C. O., Clark P. C., Greif T., Klessen R. S., 2011, MNRAS, 414, 3633

Smith R. J., Hosokawa T., Omukai K., Glover S. C. O., Klessen R. S., 2012a, MNRAS, 424, 457

Smith R. J., Iocco F., Glover S. C. O., Schleicher D. R. G., Klessen R. S., Hirano S., Yoshida N., 2012b, ApJ, submitted (arXiv: 1210.1582)

Sokasian A., Yoshida N., Abel T., Hernquist L., Springel V., 2004, MNRAS, 350, 47

Springel V., 2005, MNRAS, 364, 1105

Stacy A., Bromm V., Loeb A., 2011, MNRAS, 413, 543

Stacy A., Bromm V., Loeb A., 2011b, ApJ, 730, L1

Stacy A., Greif T. H., Bromm V., 2010, MNRAS, 403, 45

Stacy A., Greif T. H., Bromm V., 2012b, MNRAS, 422, 290

Stacy A., Greif T. H., Klessen R. S., Bromm V., Loeb A., 2012, MNRAS, submitted (arXiv:1209.1439)

Sur S., Federrath C., Schleicher D. R. G., Banerjee R., Klessen R. S., 2012, MNRAS, 423, 3148

Suwa Y., Ioka K., 2011, ApJ, 726, 107

Swartz D. A., Soria R., Tennant A. F., 2008, ApJ, 684, 282

Tan J. C., Blackman E. G., 2004, ApJ, 603, 401

Tegmark M., Silk J., Rees M. J., Blanchard A., Abel T., Palla F., 1997, ApJ, 474, 1

Tohline J. E., 2002, ARA&A, 40, 349

Tornatore L., Ferrara A., Schneider R., 2007, MNRAS, 382, 945

Turk M. J., Abel T., O'Shea B., 2009, Sci, 325, 601

Turk M. J., Clark P., Glover S. C. O., Greif T. H., Abel T., Klessen R., Bromm V., 2011, ApJ, 726, 55

Vanbeveren D., De Loore C., Van Rensbergen W., 1998, A&ARv, 9, 63

Wada K., Venkatesan A., 2003, ApJ, 591, 38

Wechsler R. H., Bullock J. S., Primack J. R., Kravtsov A. V., Dekel A., 2002, ApJ, 568, 52

Wellstein S., Langer N., Braun H., 2001, A&A, 369, 939

Whalen D., Abel T., Norman M. L., 2004, ApJ, 610, 14

Wise J. H., Abel T., 2008, ApJ, 685, 40

Woosley S. E., 1993, ApJ, 405, 273

Woosley S. E., Heger A., 2006, ApJ, 637, 914

Yoon S., Langer N., 2005, A&A, 443, 643

Yoon S.-C., Dierks A., Langer N., 2012, in press (arXiv: 201.2364)

Yoshida N., Abel T., Hernquist L., Sugiyama N., 2003, ApJ, 592, 645

Yoshida N., Omukai K., Hernquist L., 2008, Sci, 321, 669

Yoshida N., Omukai K., Hernquist L., Abel T., 2006, ApJ, 652, 6

Zhang W., Woosley S. E., Heger A., 2004, ApJ, 608, 365